Available online at www.sciencedirect.com
ScienceDirect
Advances in Space Research 42 (2008) 431–436
ADVANCES IN SPACE RESEARCH (a COSPAR publication)
www.elsevier.com/locate/asr

Resolving electrons from protons in ATIC

J. Chang [a,b,*], J.H. Adams Jr. [c], H.S. Ahn [d], G.L. Bashindzhagyan [e], K.E. Batkov [e], M. Christl [c], A.R. Fazely [f], O. Ganel [d], R.M. Gunashingha [f], T.G. Guzik [g], J. Isbert [g], K.C. Kim [d], E.N. Kouznetsov [e], Z.W. Lin [h], M.I. Panasyuk [e], A.D. Panov [e], W.K.H. Schmidt [b], E.S. Seo [d], N.V. Sokolskaya [e], John W. Watts [c], J.P. Wefel [g], J. Wu [g], V.I. Zatsepin [e]

[a] *Purple Mountain Observatory, Space Astronomy Division, Chinese Academy of Sciences, Beijing West Road 2, Nanjing, Jiangsu 210008, China*
[b] *Max-Planck Institute for Solar System Research, Katlenburg-Lindau, Germany*
[c] *Marshall Space Flight Center, Huntsville, AL, USA*
[d] *University of Maryland, Institute for Physical Science & Technology, College Park, MD, USA*
[e] *Skobeltsyn Institute of Nuclear Physics, Moscow State University, Moscow, Russia*
[f] *Southern University, Department of Physics, Baton Rouge, LA, USA*
[g] *Louisiana State University, Department of Physics and Astronomy, Baton Rouge, LA, USA*
[h] *University of Alabama, Huntsville, AL, USA*

Received 29 October 2006; received in revised form 24 May 2007; accepted 7 June 2007

Abstract

The Advanced Thin Ionization Calorimeter (ATIC) experiment is designed for high energy cosmic ray ion detection. The possibility to identify high energy primary cosmic ray electrons in the presence of the 'background' of cosmic ray protons has been studied by simulating nuclear-electromagnetic cascade showers using the FLUKA Monte Carlo simulation code. The ATIC design, consisting of a graphite target and an energy detection device, a totally active calorimeter built up of 2.5 cm × 2.5 cm × 25.0 cm BGO scintillator bars, gives sufficient information to distinguish electrons from protons. While identifying about 80% of electrons as such, only about 2 in 10,000 protons (@ 150 GeV) will mimic electrons. In September of 1999 ATIC was exposed to high-energy electron and proton beams at the CERN H2 beam line, and this data confirmed the electron detection capabilities of ATIC. From 2000-12-28 to 2001-01-13 ATIC was flown as a long duration balloon test flight from McMurdo, Antarctica, recording over 360 h of data and allowing electron separation to be confirmed in the flight data. In addition, ATIC electron detection capabilities can be checked by atmospheric gamma-ray observations.

Keywords: Electron; Simulation; Beam test; Balloon flight

1. ATIC instrument

The ATIC instrument (Guzik et al., 2004, 1999; Seo et al., 1997), shown in cross section in Fig. 1, is composed of (from the top) a pixellated Si-matrix detector, a two-layer scintillator strip hodoscope (S1), a top carbon target section of 10 cm (17.2 g/cm^2) thickness, a second scintillator hodoscope (S2), the lower carbon target (20 cm = 34.4 g/cm^2), a third scintillator hodoscope (S3), and the calorimeter made from crystals of BGO. Following the Si-matrix is the "target section" comprised of the three scintillator hodoscopes and the carbon blocks. The shower detector is a totally active ionization calorimeter that consists of 10 layers of BGO bars, each 2.5 cm by 2.5 cm in cross section and 25 cm in length. Sets of 40 such bars are arranged in 50 cm × 50 cm layers. Each layer has its

* Corresponding author. Address: Purple Mountain Observatory, Space Astronomy Division, Chinese Academy of Sciences, Beijing West Road 2, Nanjing, Jiangsu 210008, China. Tel./fax: +86 25 83332179.
E-mail address: chang@pmo.ac.cn (J. Chang).

0273-1177/$34.00 © 2007 COSPAR. Published by Elsevier Ltd. All rights reserved.
doi:10.1016/j.asr.2007.06.012

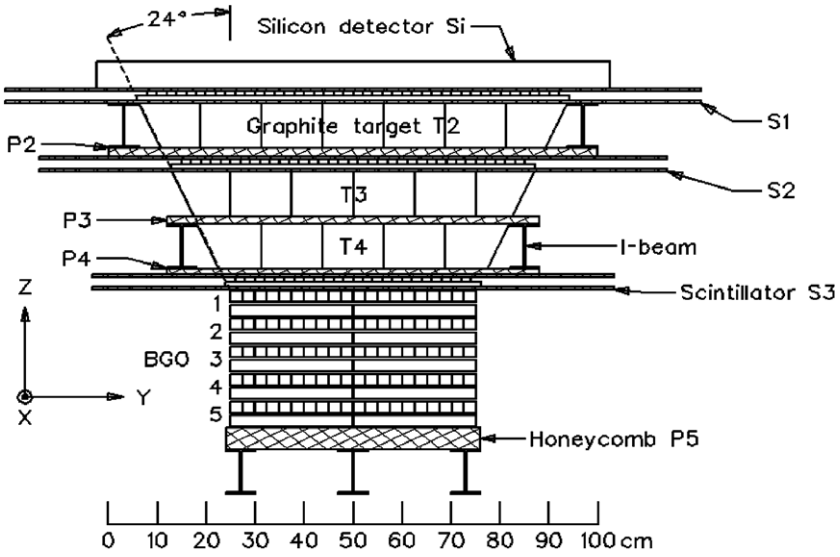

Fig. 1. A cross section of the ATIC instrument, CERN calibration configuration.

bars at right angles with respect to its neighbor(s). In this configuration, the shower is observed in three dimensions so that its axis can be reconstructed. The 2.5 cm segmentation in the BGO and 2 cm segmentation in three plastic scintillator layer pairs interleaved with the carbon layers provide resolution for the determination of the impact coordinates of the primary showering particle to better than 1 cm (Ganel et al., 2001). The calorimeter contains about 22 radiation length i.e. 25 cm of BGO that corresponds to about 1.1 interaction length. This is a good depth for the development of the electron-photon showers (from incident electrons and gamma quanta, and from gammas produced by the decay of π^0 mesons from the nuclear interaction initiated in the target), and it also provides about one interaction length in which the nuclear active products of an interaction in the target suffer more nuclear collisions.

2. Shower development in ATIC

From simulation we find that there is a large difference in shower development between electrons and protons in ATIC (Schmidt and Chang, 1999). Fig. 2 shows the difference in the shower development between electrons and protons from CERN beam test results. These are scatter plots of shower energy deposits of individual events versus widths of showers at ten different depths in the BGO calorimeter. Plotted is the energy deposit fraction (energy deposited in a specific layer divided by the total energy deposited in all layers) versus the "r.m.s." width of the showers. After determining the location of the center of energy, X_c using the crystal with the maximum energy deposit plus the crystal on either side of this one, the r.m.s. value is calculated as:

$$(\text{r.m.s.})^2 = \sum_{i=1}^{n} E_i (x_i - x_c)^2 \Big/ \sum_{i=1}^{n} E_i \qquad (1)$$

where X_c is the coordinate of the energy center; X_i is the coordinate of the center of crystal "i"; and E_i is the energy deposited in the ith crystal. The sum is over all of the crystals in an individual layer of the calorimeter. The electron events are from a run at 150 GeV and proton events are from a 375 GeV run. The 150 GeV electrons deposited, on average, about 142 GeV in the BGO calorimeter; therefore only proton events which deposited between 122 and 162 GeV in the calorimeter were used for comparison. Fig. 2 contains many more electrons than in the cosmic ray flux at these energies. However, this provides a way to study low probability events types and to assess the electron retention probability.

Fig. 3 shows the comparison of the widths of showers in the second BGO layer initiated by electrons (solid line) and protons (dashed line) events shown in Fig. 2. Fig. 3a is simulation results and Fig. 3b is beam test results. If we make use of the lateral distribution of the energy deposit in the first and second BGO layers (r.m.s.) to distinguish electron and protons, more than 95% of the protons are rejected.

As anticipated, the electron showers are significantly narrower at the top of the calorimeter than the proton showers. Proceeding deeper into the calorimeter, the electron and proton distributions overlap. The electron showers nearly "end" in the lower layers of the calorimeter and, starting at BGO-7, the two distributions again separate into two populations on the scatter plots.

Looking at the "relative gap" between the electron and proton distributions in the lower panels of Fig. 2, it is clear that a curved 'cut line' is required. We have developed an empirical function, F, to parameterize the separation. The empirical function used here is

$$F = (\text{En}/\text{Sum}) * (\text{r.m.s.})^2$$

where En is the energy deposit in BGO layer n, and Sum is the total energy deposit in all BGO layers. (En/Sum was also the ordinate value in Fig. 2.)

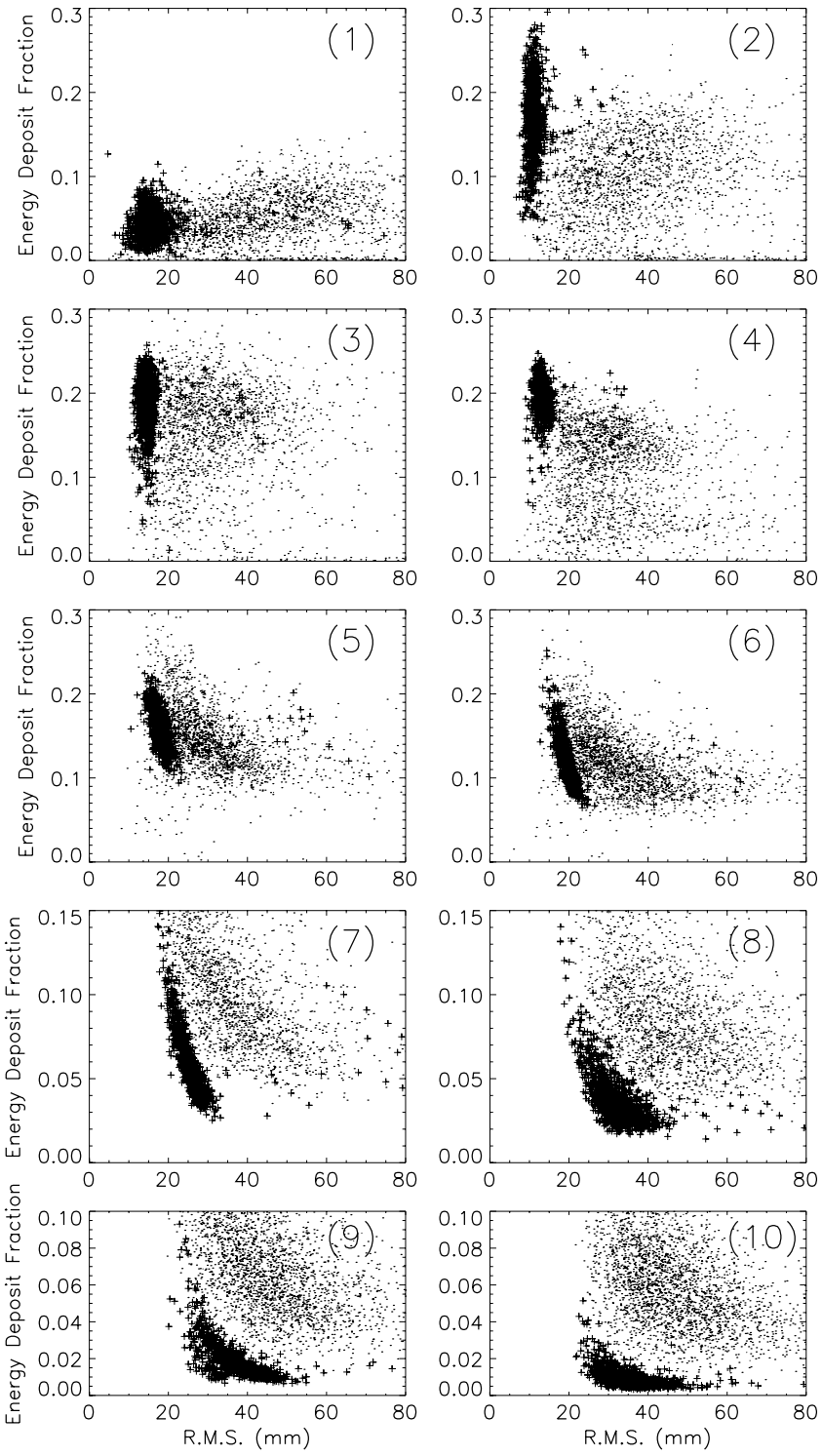

Fig. 2. Calorimeter scatter plots for electrons and protons from the CERN dataset (dark + symbols for electron events, lighter dots for proton events). Plotted is the energy deposited fraction versus the shower width (see text for details) for each layer in the calorimeter.

The F value is used to separate electrons and protons in the bottom of the BGO calorimeter, and Fig. 4 shows the F-value distribution for electrons and protons in the last BGO layer. Fig. 4a is simulation result and Fig. 4b is beam test result. The separation of the distributions of proton and electron initiated events is about as good as in Fig. 3. This again helps to suppress the proton 'background' from the point of view of electron observations. (Incidentally, using Fig. 4 alone, about 99% of the proton events would be rejected.)

In the CERN beam test, after analyzing the shower development in the top and bottom of BGO calorimeter,

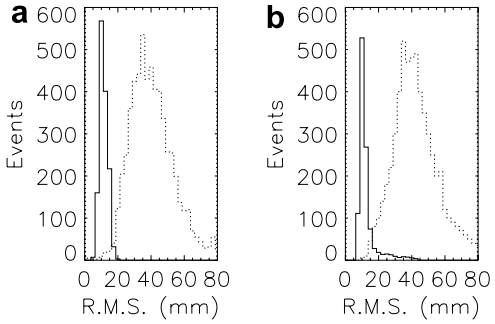

Fig. 3. Comparison of the widths of showers initiated by electrons (solid line) and protons (dashed line) as expressed by the r.m.s. value of signals in the BGO scintillator bars in the second BGO layer, BGO2: (a) simulations and (b) the CERN data.

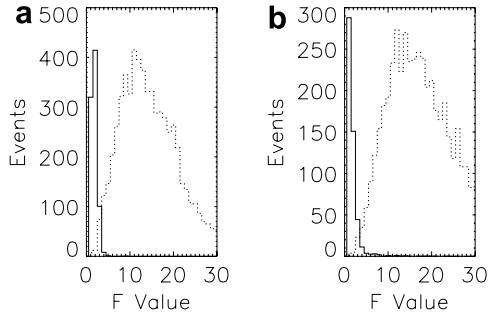

Fig. 4. *F*-value distributions for incident electrons (solid line) and incident protons of comparable total energy deposit in the calorimeter (dashed line) for the last calorimeter layer BGO10: (a) simulations, (b) CERN data.

we find only 2 in 10,000 proton events survive as background for the electron observations, while 80% of the electrons are retained.

3. Resolving electrons from protons in ATIC flight data

ATIC was launched as a long duration balloon "test" flight on 2000-12-28 from McMurdo, Antarctica (Wefel et al., 2001; Adams et al., 2001; Chang et al., 2001). During 384 h of observation time, ATIC collected 26.1 million cosmic ray events. Due to launch weight limitations at McMurdo, the balloon flight had to be carried out with only 8 BGO layers. According to simulation and CERN beam test, the 8 layer flight calorimeter should be able to separate protons and electrons as well. However, the flight data, as opposed to the CERN data, contain all allowed angles of incidence, So, we have refined the method to resolve electrons from protons in the ATIC flight data.

From simulation, we find that there is essentially no difference in the showers between gamma-ray and electron induced events in the ATIC BGO calorimeter (Chang et al., 1999). Fig. 5a shows the comparison of the widths of showers initiated by 150 GeV electrons and gamma-rays as expressed by the r.m.s. value of signals in the BGO scintillator bars in the second BGO layer. Fig. 5b shows the *F*-value distributions for 150 GeV electrons and gamma-rays in the eighth calorimeter layer. In Fig. 5 solid line is gamma-rays and dashed line is electrons. It can be seen that the distribution of electrons agrees with gamma-rays very well.

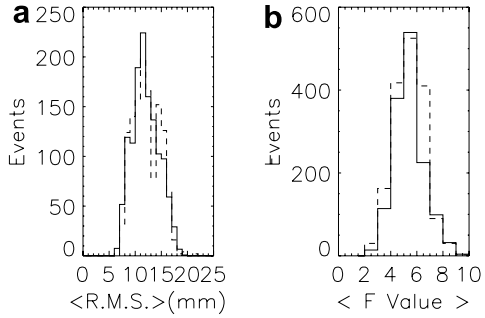

Fig. 5. Comparison of the shower development of 150 GeV electrons and gamma-rays in ATIC, solid, gamma-rays; dashed, electrons; (a) shower width distribution in the second BGO layer, (b) *F*-value distribution in the eighth BGO layer.

On the top of ATIC, there is a charge module to measure the charge of incident particles. For gamma-ray detection in ATIC, the charge module is used as an anticoincidence system in off-line data analysis. Since backscattering from the shower in the calorimeter is almost isotropic, we can choose several strips or pixels around the incident trajectory to act as anticoincidence (Adams et al., 2001). Fig. 6a shows the shower width distribution in the first plus second BGO layer for '*electron-like*' (allowing for a single charge in the charge module) events compared to the '*gamma-ray like*' (no signal in the charge module) events for energies above 50 GeV from the ATIC balloon flight data. Fig. 6b shows *F* value distribution in the seventh BGO layer plus last BGO layer for the events in the Fig. 6a. In Fig. 6 solid line is '*electron-like*' events and dashed line is '*gamma-ray like*' events. For comparison, the gamma-ray peak at the left is normalized to the electron peak. Both distributions have the same shape with a bit more proton contamination in the 'electron-like' events, as expected. However, we know that the true electron distribution should resemble the gamma-ray distribution.

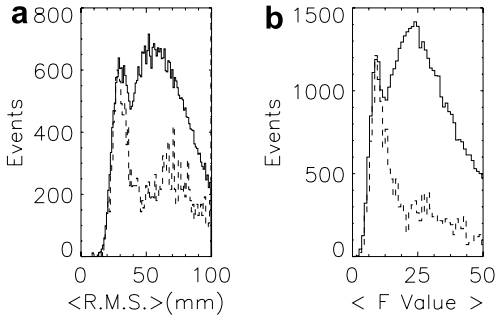

Fig. 6. (a) Shower width in the first two BGO layers, (b) *F*-value distribution in the last two BGO layers; solid line, 'electron like events'; dashed line, 'gamma-ray like events'.

4. Results

Fig. 7 shows the charge distribution observed in the Silicon matrix detector at the top of the ATIC experiment for all events with energy deposit above 50 GeV. Several features are clearly discernible, e.g. the He (alpha particle) peak and peaks around charge 6 and 8 corresponding to primary C and O nuclei, respectively. We now select the 'electron-like' events according to the gamma-ray shower development in ATIC. The dashed line after the selection shows that almost all the heavy primaries (charge above 3) have been rejected, and even the He peak cannot be found with statistical significance. We consider the He peak as particularly important for our purpose as the alpha-particle shower development, out of all heavy primaries, should show the closest resemblance to the proton shower development. In the charge distribution of 'electron-like' events, only very few counts of heavy primaries (17 out of 100,700 events) are left. (There are two more charge detectors with somewhat lower charge resolution, scintillators 1 and 2; the result from them – not shown here – look very similar to that of the silicon matrix.) This result, about 1 in 6000, is consistent with the rejection levels found in the CERN beam test.

However, we need to take into account the fact that there are differences between the showers caused by heavy ions and by protons. Principally, in a heavy ion interaction with carbon, there may be as many as twelve separate nucleon–nucleon interactions and this will lead to a wider shower profile compared to a single proton–nucleon interaction. We have studied shower development profiles with the FLUKA Monte-Carlo code and determined that the proton rejection is a factor of 8–10 below the heavy ion rejection. Thus, the heavy ion test in Fig. 7 may imply a proton rejection factor of about 1 in 600.

These results are for equal energy deposits in the calorimeter. For the eight layer ATIC flight calorimeter, an electron deposits about 85% of its energy while a proton deposits about 33% of its incident energy. So, protons that can mimic electrons start, on average, at a higher incident energy than the electrons, and there are fewer such protons due to the power-law energy spectrum.

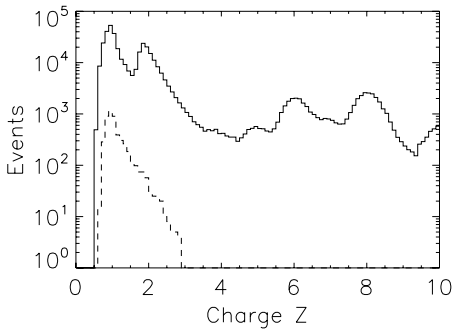

Fig. 7. Charge distribution from the Silicon matrix detector. Solid, all particles; dashed, the charge distribution after electron selection.

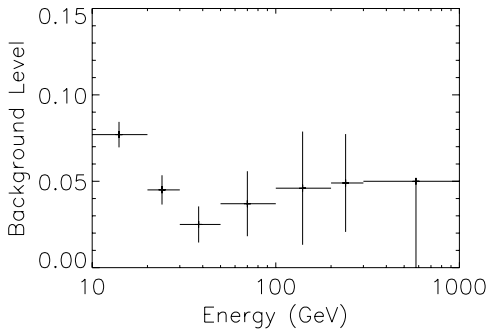

Fig. 8. The background level, proton contamination fraction within an event sample, as determined from the silicon matrix charge detector for different energies.

The events of Fig. 7 can be divided into bins according to the energy deposited in the calorimeter to investigate the dependence on energy. Correcting for the reduced proton rejection and for the spectrum, we calculate the expected background level as a function of energy (electron energy) in ATIC. The result is shown in Fig. 8. Note that there were no surviving events in the highest energy bin, so this is plotted as a limit.

It can be seen that the observed relative amount of proton admixture in the electron data (Fig. 8) does not change very much with energy, while the proton and electron fluxes spread apart. From the simulations, which cover a much wider energy range from 10 GeV to 1 TeV than the CERN measurements, we conclude that electron-proton separation seems to improve with increasing energy and therefore counteracts, somewhat, the divergence of the two spectra.

Acknowledgements

The ATIC project is funded in the US by NASA Grants NAG5-5155 (UMD), NAG5-5064 and NAG5-5306 (LSU), NAG5-5307 (SU), the Louisiana Board of Regents (LSU and SU), and the OSS R&A program (MSFC), in Russia by the Russian Foundation for Basic Research Grant 02-02-16545, and in China by the National Natural Science Foundation of China (NSFC) Grants 10573039 and BK2004220.

References

Guzik, T.G., Adams, J.H., Ahn, H.S., et al. The ATIC Collaboration, The ATIC long duration balloon project. Advances in Space Research 33, 1763, 2004.

Guzik, T.G., Adams, J.H., Ahn, H.S. et al. The ATIC Collaboration, The advanced thin ionization calorimeter (ATIC) for studies of high energy cosmic rays, in: Proceedings of 26th International Cosmic Ray Conference (Salt Lake City), vol. 5, p. 9, 1999.

Seo, E.S., Adams, J.H., Ahn, H.S., et al. The ATIC Collaboration, Advanced thin ionization calorimeter to measure ultrahigh energy cosmic rays. Advances in Space Research 19 (5), 711, 1997.

Ganel, O., Seo, E.S., Adams, J.H., et al. The ATIC Collaboration, Improving cosmic ray composition determination through better tracking. Advances in Space Research 26, 1835–1838, 2001.

Schmidt, W.K.H., Chang, J. The ATIC Collaboration, On the identification of high energy cosmic ray electrons in the advanced thin

ionization calorimeter (ATIC), in: Proceedings of 26th International Cosmic Ray Conference, Salt Lake City, vol. 5, p. 41, 1999.

Wefel, J.P., Adams, J.H., Ahn, H.S., et al. The ATIC Collaboration, The ATIC experiment: first balloon flight, in: Proceedings of 27th International Cosmic Ray Conference, Hamburg, vol. 6, p. 2111, 2001.

Adams, J.H., Ahn, H.S., Bashindzhagyan, C.L., et al. The silicon matrix as a charge detector for the ATIC experiment. Instruments and Experimental Techniques 44, 455, 2001.

Chang, J., Adams, J.H., Ahn, H.S., et al. The ATIC Collaboration, High energy electron and gamma-ray detection with ATIC, in: Proceedings of 27th International Cosmic Ray Conference, Hamburg, vol. 6, p. 2115, 2001.

Chang, J., Adams, J.H., Ahn, H.S., et al. The ATIC Collaboration, On the detection of the gamma-ray in the cosmic-ray detector, in: Proceedings of 26th International Cosmic Ray Conference, Salt Lake City, vol. 5, p. 45, 1999.